Electronic Supplementary Information

Experiment Section

Materials: Hydrochloric acid (HCl), ethylalcohol (C_2H_5OH), sodium chloride (NaCl), potassium hydroxide (KOH), and sodium carbonate (Na_2CO_3) were obtained from Chengdu Kelong Chemical Reagent Factory. Nitrate hexahydrate ($Ni(NO_3)_2·6H_2O$), and ammonium heptmolybdate ($(NH_4)_6Mo_7O_{24}·4H_2O$) were purchased from Aladdin Industrial Co. Ltd. All the reagents were used as received without further purification. Ni foam (NF) was obtained from Shenzhen Green and Creative Environmental Science and Technology Co. Ltd. Deionized water (resistivity: 18.3 MΩ·cm) used throughout experiments was purified through a Millipore system.

Synthesis of $NiMoO_4·xH_2O$/NF: In a typical synthesis process, 0.35 g $(NH_4)_6Mo_7O_{24}·4H_2O$ and 0.37 g $Ni(NO_3)_2·6H_2O$ were mixed together with 30 mL of deionized water and stirred for 20 minutes at room temperature to obtain a precursor solution. Meanwhile, NF cut into 2 cm × 3 cm were sonicated in 3 M HCl, C_2H_5OH, and deionized water, respectively for 10 min before being put into a Teflon lined autoclave along with the abovementioned precursor solution. Then autoclave was sealed and maintained at 150 °C for 6 h in an oven and then cooled down to room temperature naturally. Then the sample was taken out and thoroughly washed with deionized water and ethanol several times alternatively, then dried at 60 °C for 30 min in air.

Synthesis of $NiMoS_x$/NF: A piece of $NiMoO_4·xH_2O$/NF (2 cm × 3 cm) was immersed in 0.03 M $Na_2S·9H_2O$ solution in a Teflon-lined autoclave for the hydrothermal treatment (160 °C, 4 h). After the autoclave was cooled down naturally to room temperature, the sample was moved out, washed with deionized water and ethanol several times and dried at 60 °C for 30 min in air.

Synthesis of $NiMoS_x$@NiFe-LDH/NF: NiFe-LDH was deposited on the $NiMoS_x$/NF surface by simple electrodeposition technique. Briefly, 2.0 g $Fe(SO_4)·7H_2O$ and 2.2 g $Ni(NO_3)_2·6H_2O$ were dissolved in 50 mL deionized water and a typical three-electrode system was employed in the electrodeposition process, in which $NiMoS_x$/NF, graphite

rod and saturated calomel electrode were used as working electrode, counter electrode and reference electrode, respectively. The solution was purged with nitrogen gas for 0.5 h before the experiment. The electrodeposition was carried out at a potential of −1 V for 60 s.

Synthesis of RuO_2 or Pt/C on NF: 5 mg RuO_2 (or 20% Pt/C) was added in a solution containing 30 μL of Nafion, 485 μL of ethanol, and 485 μL of deionized water with the aid of ultrasonication (30 min) to form a homogeneous ink (5 mg mL^{-1}). 300 μL of catalyst ink was dropped onto a piece of cleaned NF (0.5 cm × 0.5 cm) with a loading mass of 1.5 mg.

Characterization: SEM (Zeiss Gemni SEM 300) and TEM (FEI TF200) were adopted to characterize the morphology and structure of as-synthesized samples. The X-ray diffraction (XRD) patterns were taken with a Rigaku Smartlab9KW diffraction system with a Cu *K*α source (λ=1.54056 Å). XPS (Thermo ESCALAB 250XI) adopting Mg as the excitation source and EDX mapping were carried out to investigate the chemical composition and element distribution of the samples.

Electrochemical measurements: Electrochemical measurements were performed with a CHI 660E electrochemical analyzer (CH Instruments, Inc., Shanghai) using a standard three electrode system using the materials supported on the substrate as working electrodes directly, a Hg/HgO with 1.0 M KOH as the inner reference electrolyte as the reference electrode, and a graphite rod as counter electrode. To exclude the influence of the oxidation peak of Ni^{2+} to Ni^{3+} on the catalytic current density in order to obtain reliable overpotential calculations, we used linear sweep voltammetry backward scans (from positive to negative direction) for the polarization curves in OER. The potentials reported in this work were converted to RHE scale via calibration with the following equation: E (vs. RHE) = E (vs. Hg/HgO) + 0.098 + 0.059 × pH. The seawater-splitting performance of the electrolyzers were tested in a two-electrode system, where OER electrodes are as the anode and HER electrodes as the cathode. Three different electrolytes, including 1 M KOH, 1 M KOH + 0.5 M NaCl, and 1 M KOH + seawater, were used, and the pH was about 14. All the LSV

curves were iR compensated. EIS was obtained at the open circuit potential from 10000 to 0.01 Hz at an amplitude of 5 mV.

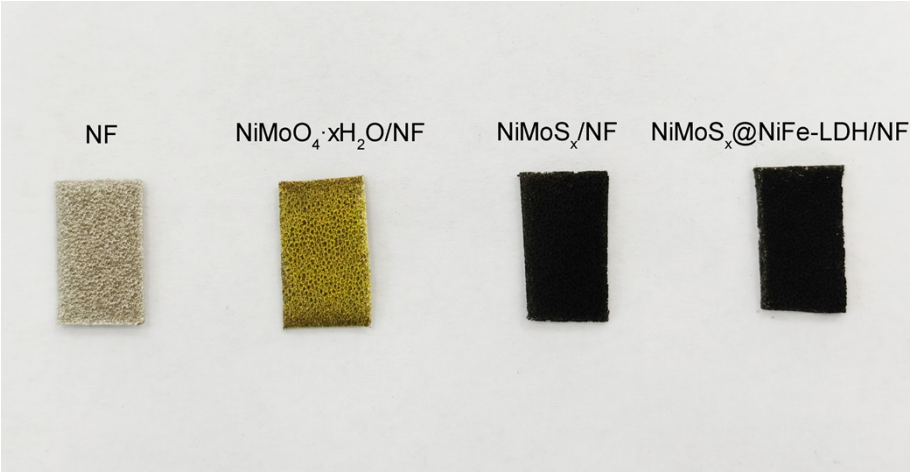

Fig. S1. Optical photograph of NF, $NiMoO_4 \cdot xH_2O$/NF, $NiMoS_x$/NF, and $NiMoS_x$@NiFe-LDH/NF.

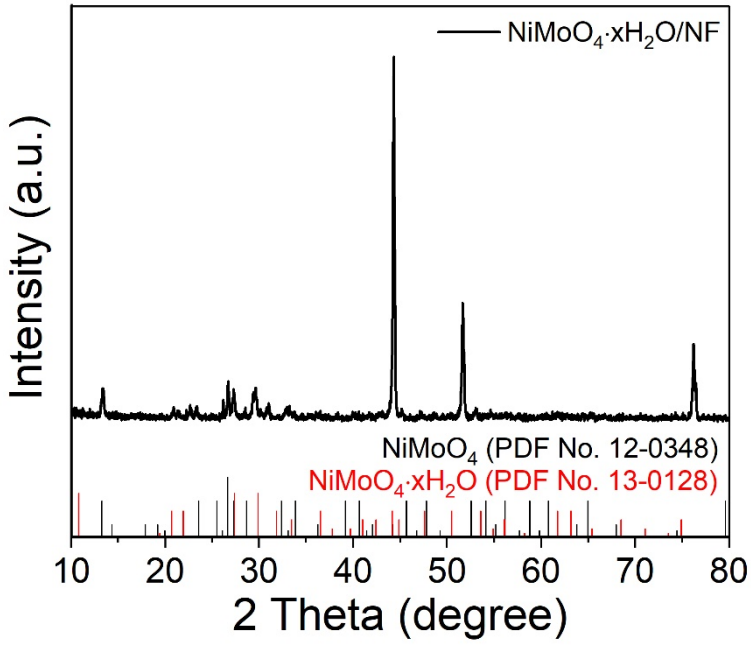

Fig. S2. XRD pattern of $NiMoO_4 \cdot xH_2O$/NF.

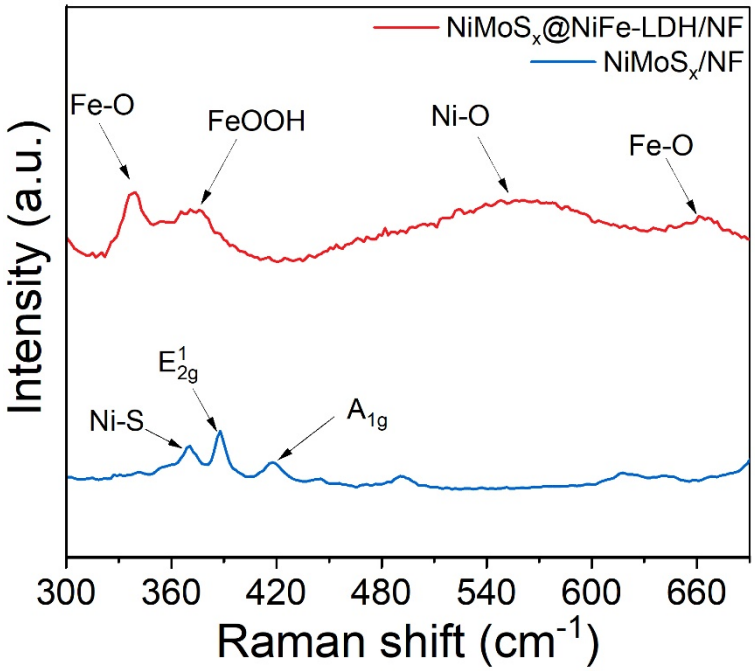

Fig. S3. Raman spectra of $NiMoS_x$/NF and $NiMoS_x$@NiFe-LDH/NF.

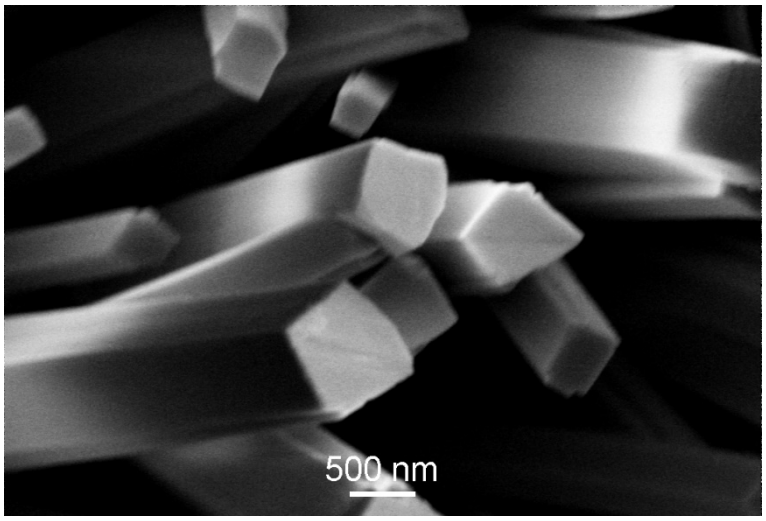

Fig. S4. SEM image of $NiMoO_4 \cdot xH_2O$/NF.

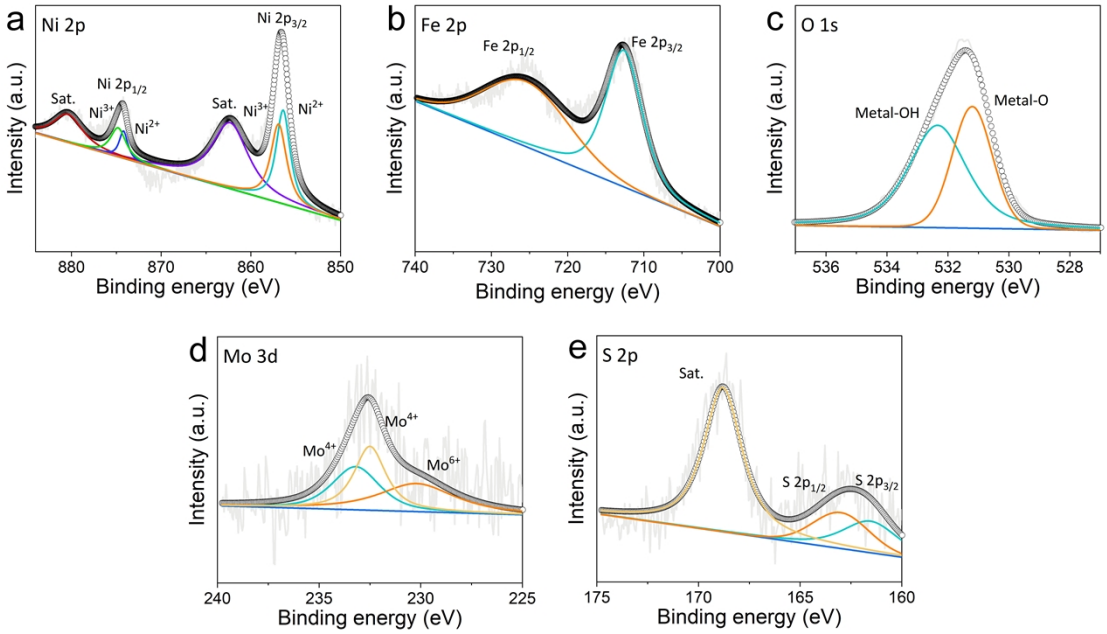

Fig. S5. High-resolution XPS spectra for $NiMoS_x$@NiFe-LDH/NF in the (a) Ni 2p, (b) Fe 2p, (c) O 1s, (d) Mo 3d, and (e) S 2p regions.

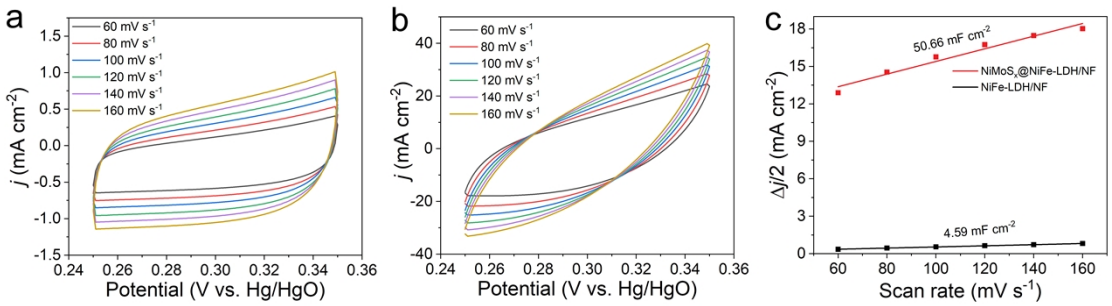

Fig. S6. Cyclic voltammetry curves for (a) NiFe-LDH/NF and (b) $NiMoS_x$@NiFe-LDH/NF in the double layer region at different scan rates of 60, 80, 100, 120, 140, and 160 mV s^{-1} in 1 M KOH. (c) Capacitive current densities of NiFe-LDH/NF and $NiMoS_x$@NiFe-LDH/NF at 0.30 V vs. Hg/HgO as a function of the scan rate.

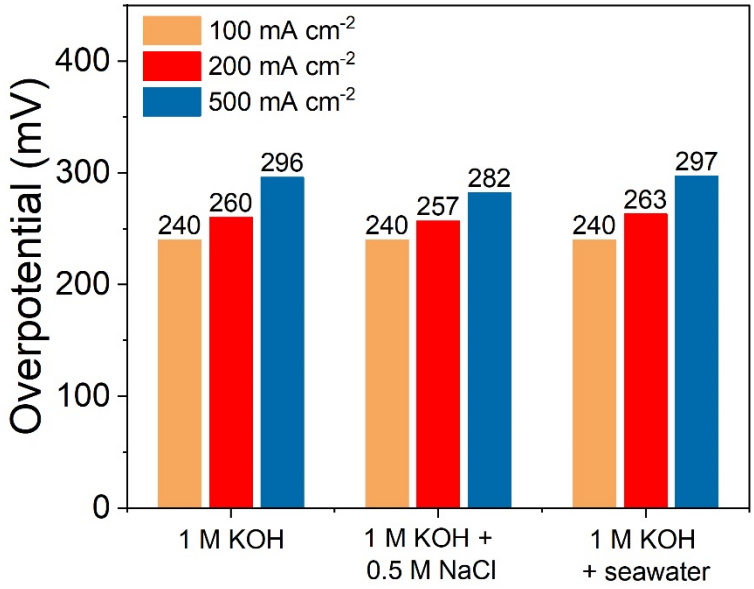

Fig. S7. Overpotential comparison of $NiMoS_x$@NiFe-LDH/NF for OER in 1 M KOH, 1 M KOH + 0.5 M NaCl, and 1 M KOH + seawater.

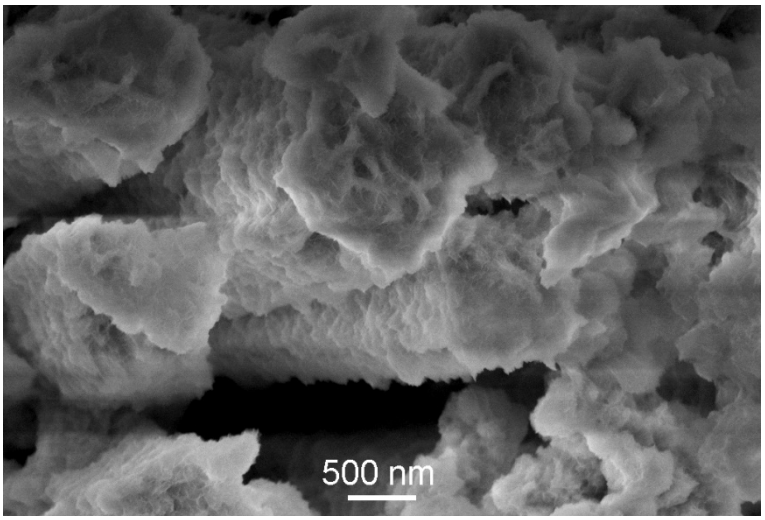

Fig. S8. SEM image of $NiMoS_x$@NiFe-LDH/NF after durability test in 1 M KOH + seawater solution.

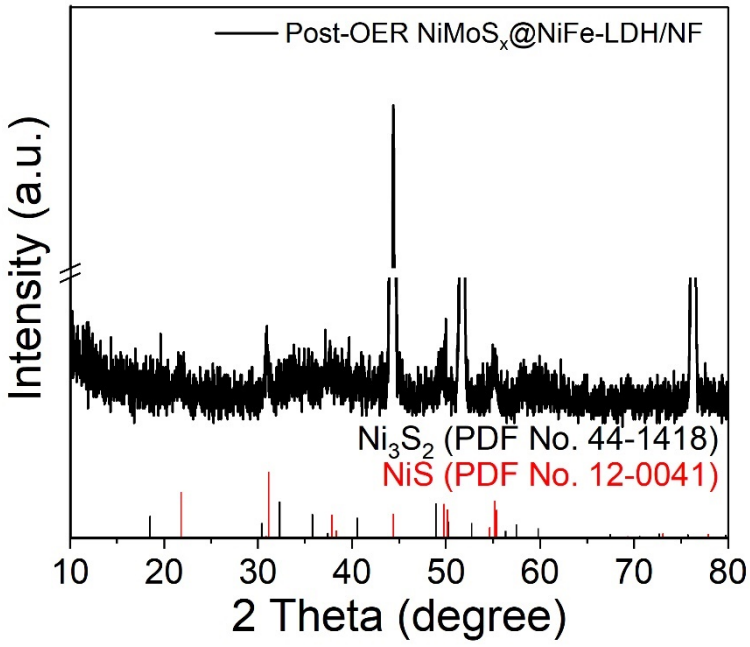

Fig. S9. XRD pattern of $NiMoS_x$@NiFe-LDH/NF after durability test in 1 M KOH + seawater solution.

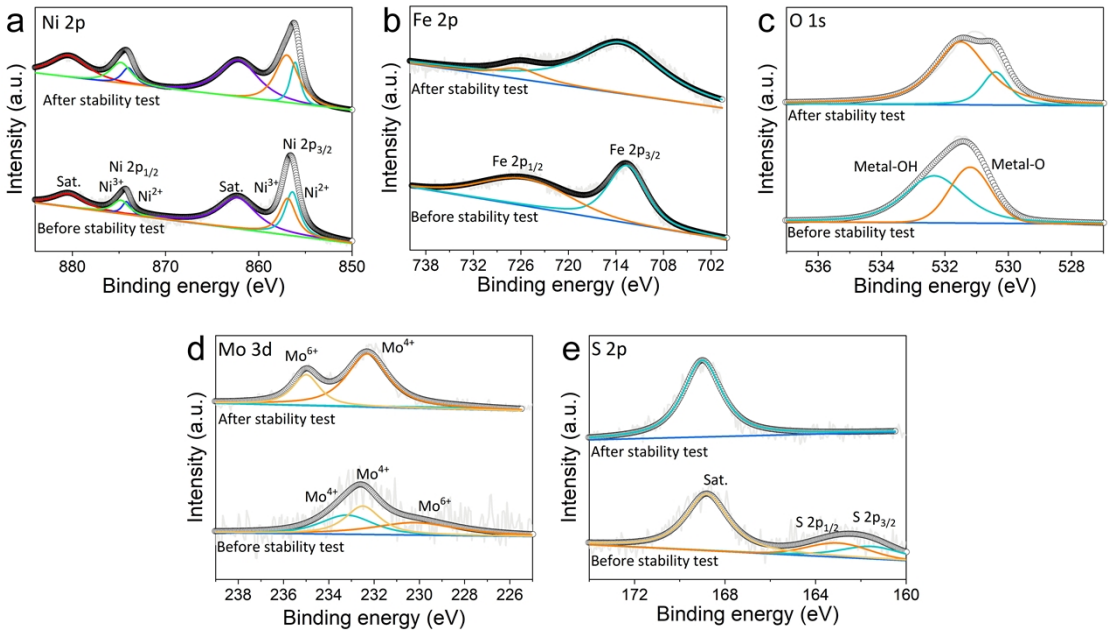

Fig. S10. High-resolution XPS spectra for $NiMoS_x$@NiFe-LDH/NF in the (a) Ni 2p, (b) Fe 2p, (c) O 1s, (d) Mo 3d, and (e) S 2p regions before and after durability test in 1 M KOH + seawater solution.

As shown in the high-resolution spectrum of O 1s (Fig. S10c), after durabilty test, the content of mental-OH is significantly increased and the the sulfide surface was oxidized (Fig. S10e).

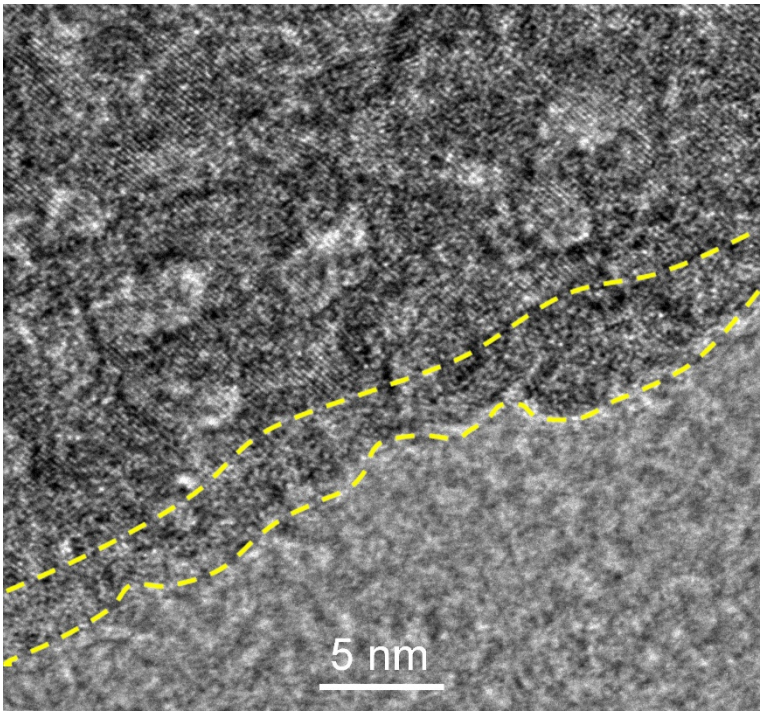

Fig. S11. HRTEM image of $NiMoS_x$@NiFe-LDH after durability test in 1 M KOH + seawater solution.

From the HRTEM image of $NiMoS_x$@NiFe-LDH after durability test in 1 M KOH + seawater solution, we can observe that the $NiMoS_x$@NiFe-LDH consists of both crystalline and amorphous parts, generating rich crystalline-amorphous boundaries, which may provide more catalytically active sites for OER.

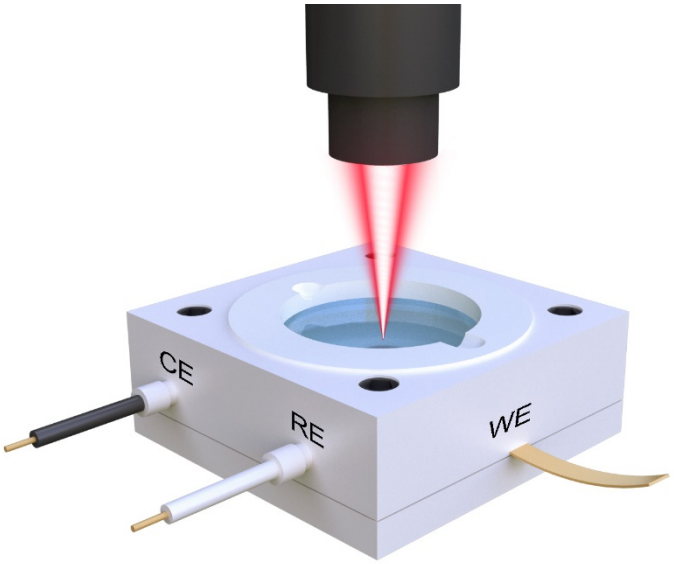

Fig. S12. Schematic of in-situ electrochemical Raman cell.

In-situ Raman spectra were acquired by confocal Raman spectroscopy (Horiba Jobin Yvon Co., France) under controlled potential, and a 633 nm laser was used as the excitation source. The electrochemical cell was made of quartz and stood in front of the objective. The $NiMoS_x$@NiFe-LDH/NF or NiFe-LDH/NF served as the working electrode and the laser shined through a quartz window onto the working electrode surface. Graphite rod and Ag/AgCl electrode were used as the counter electrode and reference electrode, respectively. 0.1 M KOH + seawater was used as the electrolyte. Each Raman spectrum was collected with an acquisition time of 10 s with 5-10 sweeps from 200 to 1000 cm^{-1} under current-time measurement at a constant potential using a confocal Raman microscope coupled with an Olympus 50 × LDW objective.

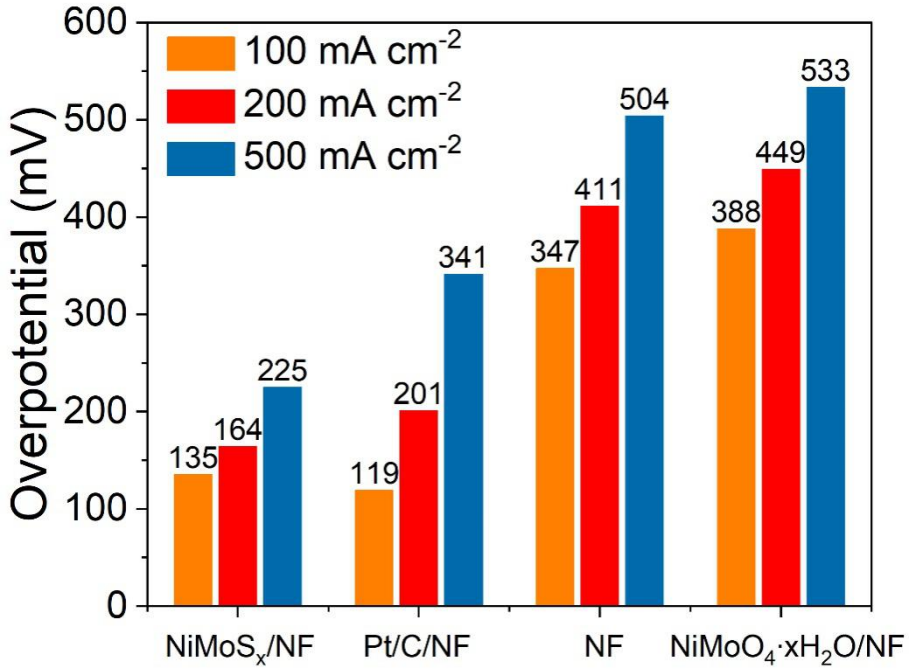

Fig. S13. Overpotential comparison of $NiMoS_x$/NF, Pt/C/NF, NF, and $NiMoO_4 \cdot xH_2O$/NF for HER in 1 M KOH.

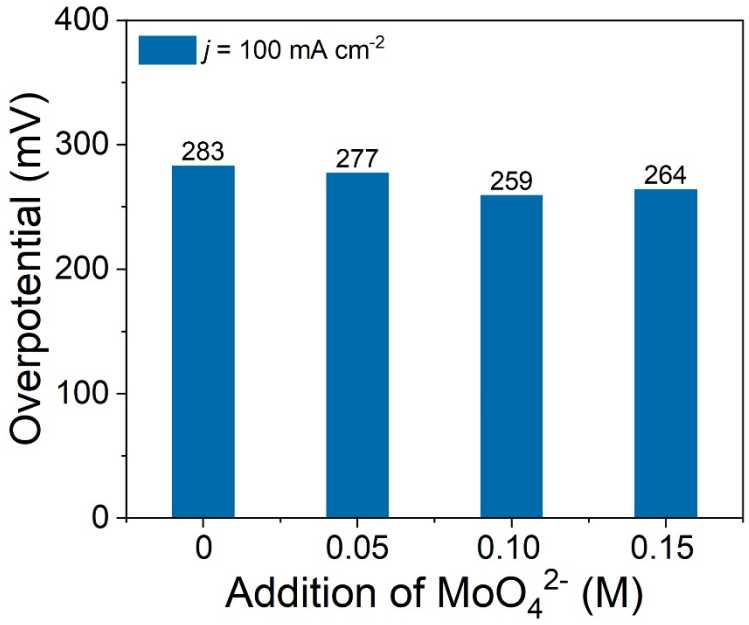

Fig. S14. Overpotential comparison of $NiMoS_x$/NF at 100 mA cm^{-2} with the addition of different concentration of MoO_4^{2-} in alkaline seawater.

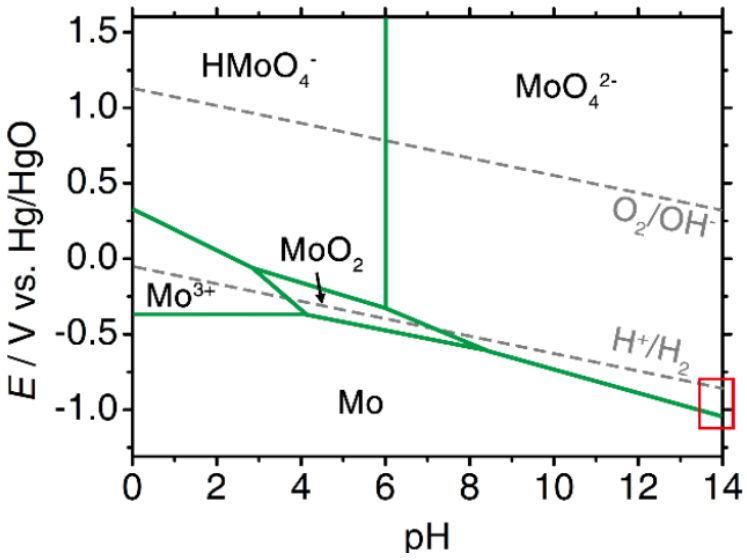

Fig. S15. Pourbaix diagram of Mo in water.[1-3]

The concentration of soluble species is 1.0×10^{-6} mol kg^{-1}. The red boxed area shows the more negative reduction potential of MoO_4^{2-} than hydrogen evolution.

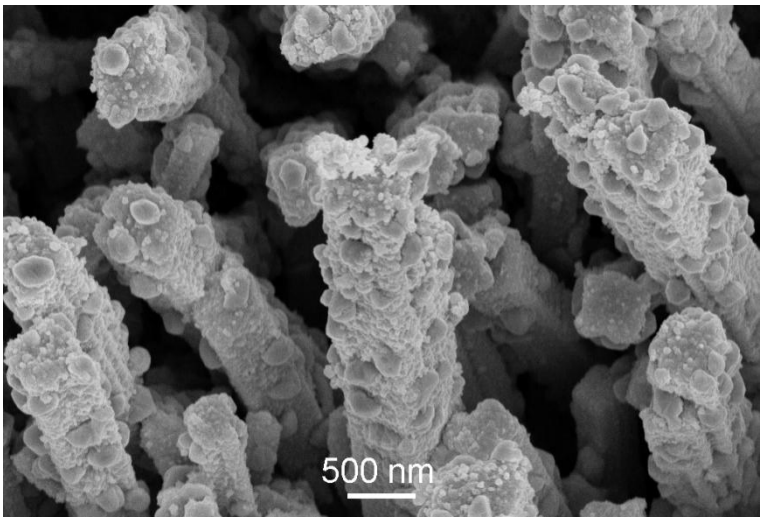

Fig. S16. SEM image of $NiMoS_x$/NF after durability test in 1 M KOH + seawater solution.

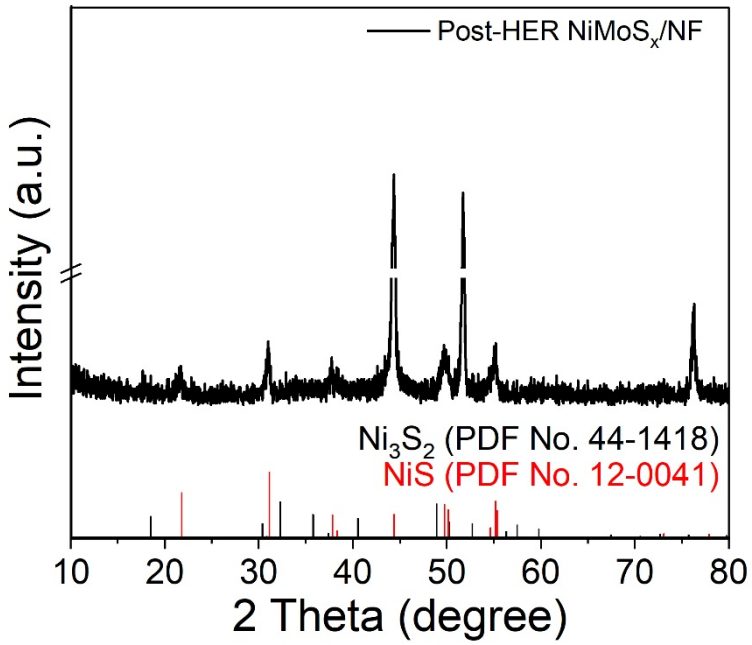

Fig. S17. XRD pattern of $NiMoS_x$/NF after durability test in 1 M KOH + seawater solution.

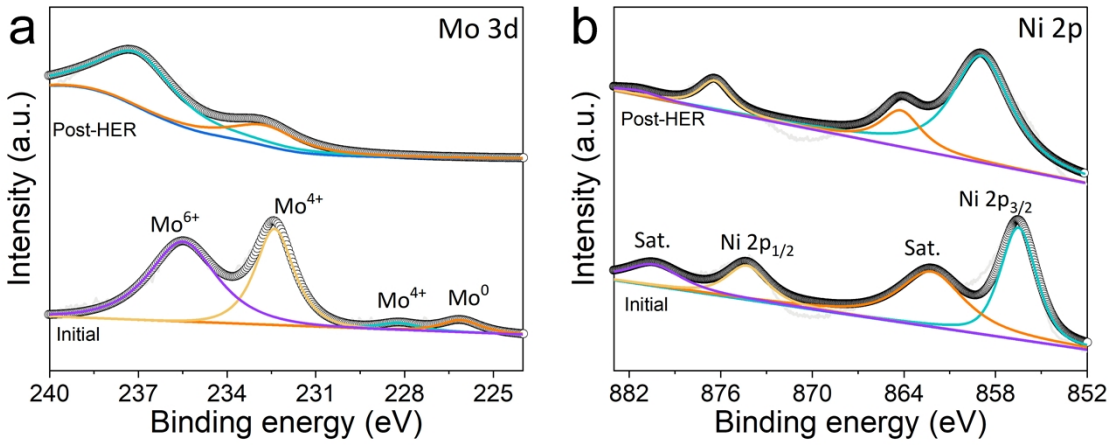

Fig. S18. High-resolution XPS spectra for $NiMoS_x$/NF in the (a) Mo 3d and (b) Ni 2p regions before and after HER test in 1 M KOH + seawater solution.

Table S1. Comparison of OER performances for $NiMoS_x$@NiFe-LDH/NF with recently reported self-supported electrocatalysts in alkaline seawater.

Electrocatalyst	Electrolyte	η_{500}* (mV)	Testing time	Ref.
$NiMoS_x$@NiFe-LDH/NF	1 M KOH + seawater	297	500 h@500 mA cm^{-2}	This work
NiMoN@NiFeN/NF	1 M KOH + seawater	369	24 h@500 mA cm^{-2}	4
S-Ni/Fe(OOH)/NF	1 M KOH + seawater	398	100 h@100 mA cm^{-2}	5
Fe_2O_3/NiO/NF	1 M KOH + seawater	523	50 h@100 mA cm^{-2}	6
CoP_x@FeOOH/NF	1 M KOH + seawater	337	80 h@500 mA cm^{-2}	7
BZ-NiFe-LDH/CC	1 M KOH + seawater	610	100 h@500 mA cm^{-2}	8
Ni_2P-Fe_2P/NF	1 M KOH + seawater	385	36 h@500 mA cm^{-2}	9
Fe-NiSOH/NF	1 M KOH + seawater	311	900 h@500 mA cm^{-2}	10
NiFe/NiS_x-NF (Ni^3)	1 M KOH + seawater	350	12 h@400 mA cm^{-2}	11
NF/NiFe LDH	1 M KOH + seawater	296	100 h@200 mA cm^{-2}	12
Ni_3S_2/Fe-NiP_x/NF	1 M KOH + seawater	336	30 h@200 mA cm^{-2}	13
AC-Fe(O)OH/NF	1 M KOH + seawater	340	100 h@200 mA cm^{-2}	14
Ag/NiFe LDH/NF	1 M KOH + seawater	279	1000 h@1000 mA cm^{-2}	15
NiCoS/NF	1 M KOH + seawater	440	100 h@100 mA cm^{-2}	16
HMIL-88@PPy-TA/NF	1 M KOH + seawater	345	100 h@100 mA cm^{-2}	17

η_{500}* represent the overpotentials required to attain j of 500 mA cm^{-2}.

Table S2. Comparison of HER performances for $NiMoS_x$/NF with recently reported self-supported electrocatalysts in alkaline seawater.

Electrocatalyst	Electrolyte	η_{100}* (mV)	Testing time	Ref.
$NiMoS_x$/NF	1 M KOH + seawater	141	400 h@500 mA cm^{-2}	This work
NiMoN/NF	1 M KOH + seawater	56	24 h@500 mA cm^{-2}	4
CoP_x/NF	1 M KOH + seawater	190	80 h@500 mA cm^{-2}	7
Ni_2P-Fe_2P/NF	1 M KOH + seawater	252	40 h@500 mA cm^{-2}	9
NiFeS/NF	1 M KOH + seawater	217	25 h@500 mA cm^{-2}	18
S-$NiMoO_4$@NiFe-LDH/NF	1 M KOH + seawater	220	20 h@20 mA cm^{-2}	19
NiPS/NF	1 M KOH + seawater	188	24 h@250 mA cm^{-2}	20
FeS/iron foam	1 M KOH + seawater	225	300 h@1000 mA cm^{-2}	21
MoS_2-$(FeNi)_9S_8$/Ni-Fe Foam	1 M KOH + seawater	164	70 h@50 mA cm^{-2}	22
Ni_3S_2-MoS_2-Ni_3S_2/NF	1 M KOH + 0.5 M NaCl	188	50 h@100 mA cm^{-2}	23
$Ni_3Bi_2S_2$/NF	1 M KOH + 0.5 M NaCl	157	24 h@500 mA cm^{-2}	24
Ni/V_2O_3/NF	1 M KOH + 0.5 M NaCl	430	24 h@1000 mA cm^{-2}	25

η_{100}* represent the overpotentials required to attain j of 100 mA cm^{-2}.

Table S3. Comparison of overall-seawater splitting performance of $NiMoS_x$@NiFe-LDH/NF||$NiMoS_x$/NF with recently reported electrocatalysts under alkaline conditions.

Electrolyzer	Electrolyte	V_{100}* (V)	V_{500}* (V)	Testing time	Ref.
$NiMoS_x$@NiFe-LDH/NF||$NiMoS_x$/NF	1 M KOH + seawater	1.61	1.84	150 h@500 mA cm^{-2}	This work
NiMoN/NF||NiMoN@NiFeN/NF	1 M KOH + seawater	1.58	1.77	100 h@500 mA cm^{-2}	4
S-(Ni,Fe)OOH/NF||NiMoN/NF	1 M KOH + seawater	1.62	1.74	100 h@500 mA cm^{-2}	5
CoP_x/NF||CoP_x@FeOOH/NF	1 M KOH + seawater	1.71	1.87	80 h@500 mA cm^{-2}	7
Ni_2P-Fe_2P||Ni_2P-Fe_2P	1 M KOH + seawater	1.81	2.04	38 h@500 mA cm^{-2}	9
NiFe/NiS_x/NF||Ni-NiO-Cr_2O_3/NF	1 M KOH + seawater	1.82	~2.2	500 h@1000 mA cm^{-2}	11
NiPS/NF||NiPS/NF	1 M KOH + seawater	1.68	/	60 h@200 mA cm^{-2}	20
Ni_3S_2-MoS_2-Ni_3S_2/NF|| Ni_3S_2-MoS_2-Ni_3S_2/NF	1 M KOH + seawater	1.82	/	100 h@100 mA cm^{-2}	23
Ni_3N@C/NF||Ni_3FeN@C/NF	1 M KOH + seawater	1.69	1.91	100 h@100 mA cm^{-2}	26
NiCoHPi@Ni_3N/NF|| NiCoHPi@Ni_3N/NF	1 M KOH + seawater	1.86	1.99	40 h@200 mA cm^{-2}	27
NiCoP/NiCo-LDH/NF|| NiCoP/NiCo-LDH/NF	1 M KOH + seawater	1.66	/	50 h@15 mA cm^{-2}	28
Co-Fe_2P/NF||Co-Fe_2P/NF	1 M KOH + seawater	1.69	/	24 h@100 mA cm^{-2}	29
Mo-NiFe-PO_3/NFF|| Mo-NiFe-PO_3/NFF	1 M KOH + 0.5 M NaCl	1.65	/	100 h@500 mA cm^{-2}	30
S,P-(Ni,Mo,Fe)OOH/NiMoP|| S,P-(Ni,Mo,Fe)OOH/NiMoP	1 M KOH + 0.5 M NaCl	1.72	/	20 h@100 mA cm^{-2}	31
RuNi-Fe_2O_3/IF||RuNi-Fe_2O_3/IF	1 M KOH + 0.5 M NaCl	1.73	/	100 h@100 mA cm^{-2}	32
MIL-(IrNiFe)@NF|| MIL-(IrNiFe)@NF	1 M KOH + 0.5 M NaCl	1.67	1.9	12 h@500 mA cm^{-2}	33

V_{100}* and V_{500}* represent the voltages required to attain *j* of 100 and 500 mA cm^{-2}, respectively.

References

1 V. S. Saji and C.-W. Lee, Molybdenum, molybdenum oxides, and their electrochemistry, *ChemSusChem,* 2012, **5**, 1146–1161.

2 M. Nishimoto, I. Muto and Y. Sugawara, N. Hara, Morphological characteristics of trenching around MnS inclusions in type 316 stainless steel: the role of molybdenum in pitting corrosion resistance, *J. Electrochem. Soc.,* 2019, **166**, C3081.

3 W. Du, Y. Shi, W. Zhou, Y. Yu and B. Zhang, Unveiling the in situ dissolution and polymerization of Mo in Ni_4Mo alloy for promoting the hydrogen evolution reaction, *Angew. Chem., Int. Ed.,* 2021, **60**, 7051–7055.

4 L. Yu, Q. Zhu, S. Song, B. McElhenny, D. Wang, C. Wu, Z. Qin, J. Bao, Y. Yu, S. Chen and Z. Ren, Non-noble metal-nitride based electrocatalysts for high-performance alkaline seawater electrolysis, *Nat. Commun.,* 2019, **10**, 5106.

5 L. Yu, L. Wu, B. McElhenny, S. Song, D. Luo, F. Zhang, Y. Yu, S. Chen and Z. Ren, Ultrafast room-temperature synthesis of porous S-doped Ni/Fe (oxy)hydroxide electrodes for oxygen evolution catalysis in seawater splitting, *Energy Environ. Sci.,* 2020, **13**, 3439–3446.

6 L. Li, G. Zhang, B. Wang, D. Zhu, D. Liu, Y. Liu and S. Yang, Fe_2O_3/NiO interface for the electrochemical oxygen evolution in seawater and domestic sewage, *ACS Appl. Mater. Interfaces,* 2021, **13**, 37152–37161.

7 L. Wu, L. Yu, B. McElhenny, X. Xing, D. Luo, F. Zhang, J. Bao, S. Chen and Z. Ren, Rational design of core-shell-structured CoP_x@FeOOH for efficient seawater electrolysis, *Appl. Catal. B: Environ.,* 2021, **294**, 120256.

8 L. Zhang, J. Liang, L. Yue, K. Dong, J. Li, D. Zhao, Z. Li, S. Sun, Y. Luo, Q. Liu, G. Cui, A. Ali Alshehri, X. Guo and X. Sun, Benzoate anions-intercalated NiFe-layered double hydroxide nanosheet array with enhanced stability for electrochemical seawater oxidation, *Nano Res. Energy,* 2022, **1**, e9120028.

9 L. Wu, L. Yu, F. Zhang, B. McElhenny, D. Luo, A. Karim, S. Chen and Z. Ren, Heterogeneous bimetallic phosphide Ni_2P-Fe_2P as an efficient bifunctional catalyst for water/seawater splitting, *Adv. Funct. Mater.,* 2021, **31**, 2006484.

10 C. Huang, Q. Zhou, D. Duan, L. Yu, W. Zhang, Z. Wang, J. Liu, B. Peng, P. An, J. Zhang, L. Li, J. Yu and Y. Yu, The rapid self-reconstruction of Fe-modified Ni hydroxysulfide for efficient and stable large-current-density water/seawater oxidation, *Energy Environ. Sci.,* 2022, **15**, 4647–4658.

11 Y. Kuang, M. J. Kenney, Y. Meng, W.-H. Hung, Y. Liu, J. E. Huang, R. Prasanna, P. Li, Y. Li, L. Wang, M.-C. Lin, M. D. McGehee, X. Sun and H. Dai, Solar-driven, highly sustained splitting of seawater into hydrogen and oxygen fuels, *Proc. Natl. Acad. Sci. U. S. A.,* 2019, **116**, 6624–6629.

12 M. Ning, L. Wu, F. Zhang, D. Wang, S. Song, T. Tong, J. Bao, S. Chen, L. Yu and Z. Ren, One-step spontaneous growth of NiFe layered double hydroxide at room temperature for seawater oxygen evolution, *Mater. Today Phys.,* 2021, **19**, 100419.

13 X. Luo, P. Ji, P. Wang, X. Tan, L. Chen and S. Mu, Spherical Ni_3S_2/Fe-NiP_x magic cube with ultrahigh water/seawater oxidation efficiency, *Adv. Sci.,* 2022, **9**, 2104846.

14 R.-Y. Fan, X.-Y. Zhang, N. Yu, F.-G. Wang, H.-Y. Zhao, X. Liu, Q.-X. Lv, D.-P. Liu, Y.-M. Chai and B. Dong, Rapid "self-healing" behavior induced by chloride anions to renew the Fe-Ni(oxy)hydroxide surface for long-term alkaline seawater electrolysis, *Inorg. Chem. Front.,* 2022, **9**, 4216–4224.

15 S. Liu, S. Ren, R.-T. Gao, X. Liu and L. Wang, Atomically embedded Ag on transition metal hydroxides triggers the lattice oxygen towards sustained seawater electrolysis, *Nano Energy,* 2022, **98**, 107212.

16 C. Wang, M. Zhu, Z. Cao, P. Zhu, Y. Cao, X. Xu, C. Xu and Z. Yin, Heterogeneous bimetallic sulfides based seawater electrolysis towards stable industrial-level large current density, *Appl. Catal. B: Environ.,* 2021, **291**, 120071.

17 Y. Chen, L. Shen, C. Wang, S. Feng, N. Zhang, K. Zhang and B. Yang, Utilizing tannic acid and polypyrrle to induce reconstruction to optimize the activity of MOF-derived electrocatalyst for water oxidation in seawater, *Chem. Eng. J.,* 2022, **430**, 132632.

18 J. Chen, L. Zhang, J. Li, X. He, Y. Zheng, S. Sun, X. Fang, D. Zheng, Y. Luo, Y. Wang, J. Zhang, L. Xie, Z. Cai, Y. Sun, A. A. Alshehri, Q. Kong, C. Tang and X. Sun, High-efficiency overall alkaline seawater splitting: using a nickel-iron sulfide nanosheet array as a bifunctional electrocatalyst, *J. Mater. Chem. A,* 2023, **11**, 1116–1122.

19 H. Wang, L. Chen, L. Tan, X. Liu, Y. Wen, W. Hou and T. Zhan, Electrodeposition of NiFe-layered double hydroxide layer on sulfur-modified nickel molybdate nanorods for highly efficient seawater splitting, *J. Colloid Interface Sci.,* 2022, **613**, 349–358.

20 H.-Y. Wang, J.-T. Ren, L. Wang, M.-L. Sun, H.-M. Yang, X.-W. Lv and Z.-Y. Yuan, Synergistically enhanced activity and stability of bifunctional nickel phosphide/sulfide heterointerface electrodes for direct alkaline seawater electrolysis, *J. Energy Chem.,* 2022, **75**, 66–73.

21 H. Lv, C. Fu, J. Fan, Y. Zhang and W. Hao, Mild construction of robust FeS-based electrode for pH-universal hydrogen evolution at industrial current density, *J. Colloid Interface Sci.,* 2022, **626**, 384–394.

22 S. Song, Y. Wang, S. Zhou, H. Gao, X. Tian, Y. Yuan, W. Li and J. Zang, One-step synthesis of heterostructural MoS_2-$(FeNi)_9S_8$ on Ni-Fe foam synergistically boosting for efficient fresh/seawater electrolysis, *ACS Appl. Energy Mater.,* 2022, **5**, 1810–1821.

23 Y. Li, X. Wu, J. Wang, H. Wei, S. Zhang, S. Zhu, Z. Li, S. Wu, H. Jiang and Y. Liang, Sandwich structured Ni_3S_2-MoS_2-Ni_3S_2@Ni foam electrode as a stable bifunctional electrocatalyst for highly sustained overall seawater splitting, *Electrochim. Acta,* 2021, **390**, 138833.

24 D. Yao, W. Hao, S. Weng, M. Hou, W. Cen, G. Li, Z. Chen and Y. Li, Local photothermal effect enabling $Ni_3Bi_2S_2$ nanoarray efficient water electrolysis at large current density, *Small,* 2022, **18**, 2106868.

25 G. Liu, H. Lv, Q. Quan, X. Li, H. Lu, W. Li, X. Cui and L. Jiang, Self-powered electrolysis systems for sustainable hydrogen generation from natural seawater via a Ni/V_2O_3 Schottky electrode, *Chem. Eng. J.,* 2022, **450**, 138079.

26 B. Wang, M. Lu, D. Chen, Q. Zhang, W. Wang, Y. Kang, Z. Fang, G. Pang and S. Feng, Ni_xFe_yN@C microsheet arrays on Ni foam as an efficient and durable electrocatalyst for electrolytic splitting of alkaline seawater, *J. Mater. Chem. A,* 2021, **9**, 13562–13569.

27 H. Sun, J. Sun, Y. Song, Y. Zhang, Y. Qiu, M. Sun, X. Tian, C. Li, Z. Lv and L. Zhang, Nickel-cobalt hydrogen phosphate on nickel nitride supported on nickel foam for alkaline seawater electrolysis, *ACS Appl. Mater. Interfaces,* 2022, **14**, 22061–22070.

28 Y. Wu, Z. Tian, S. Yuan, Z. Qi, Y. Feng, Y. Wang, R. Huang, Y. Zhao, J. Sun, W. Zhao, W. Guo, J. Feng and J. Sun, Solar-driven self-powered alkaline seawater electrolysis via multifunctional earth-abundant heterostructures, *Chem. Eng. J.,* 2021, **411**, 128538.

29 S. Wang, P. Yang, X. Sun, H. Xing, J. Hu, P. Chen, Z. Cui, W. Zhu and Z. Ma, Synthesis of 3D heterostructure Co-doped Fe_2P electrocatalyst for overall seawater electrolysis, *Appl. Catal. B: Environ.,* 2021, **297**, 120386.

30 S. Song, Y. Wang, X. Liu, X. Tian, Y. Liu, X. Liu, F. Sun, Y. Yuan, W. Li and J. Zang, Synthesis of Mo-doped NiFe-phosphate hollow bird-nest architecture for efficient and stable seawater electrolysis, *Appl. Surf. Sci.,* 2022, **604**, 154588.

31 H. Chen, Y. Zou, J. Li, K. Zhang, Y. Xia, B. Hui and D. Yang, Wood aerogel-derived sandwich-like layered nanoelectrodes for alkaline overall seawater electrosplitting, *Appl. Catal. B: Environ.,* 2021, **293**, 120215.

32 T. Cui, X. Zhai, L. Guo, J.-Q. Chi, Y. Zhang, J. Zhu, X. Sun and L. Wang, Controllable synthesis of a self-assembled ultralow Ru, Ni-doped Fe_2O_3 lily as a bifunctional electrocatalyst for large-current-density alkaline seawater electrolysis, *Chin. J. Catal.,* 2022, **43**, 2202–2211.

33 X. Zhai, Q. Yu, G. Liu, J. Bi, Y. Zhang, J. Chi, J. Lai, B. Yang and L. Wang, Hierarchical microsphere MOF arrays with ultralow Ir doping for efficient hydrogen evolution coupled with hydrazine oxidation in seawater, *J. Mater. Chem. A,* 2021, **9**, 27424–27433.